The International Journal of Advanced Manufacturing Technology (2019) 100:623–635
https://doi.org/10.1007/s00170-018-2728-9

ORIGINAL ARTICLE

Effect of lay-up configuration and processing parameters on surface quality during fiber laser cutting of CFRP laminates

Maojun Li[1] · Shuo Li[1] · Xujing Yang[1] · Yi Zhang[1,2] · Zhichao Liang[1,2]

Received: 15 March 2018 / Accepted: 17 September 2018 / Published online: 27 September 2018

Abstract
Experimental data is presented relating to heat-affected zone (HAZ) and surface quality when using continuous wave (CW) fiber laser cutting carbon fiber reinforced plastic (CFRP) with varying configurations including + 45°/− 45°, 0°/90°, and plain woven. The effect of typical cutting parameters including laser power, cutting speed, and assist gas pressure on laser cutting quality of different type of workpiece materials was investigated. A full factorial experimental array was employed involving 24 trials. The statistical significance of individual cutting parameters was determined using main effects plot together with ANOVA. Results showed that the fiber laser was feasible for cutting CFRP with very high efficiency. The HAZ level of laser cutting CFRP was highly related to fiber orientation, laser power, and cutting speed based on theoretical and statistical analysis. Thermal model was built to simulate HAZ values recorded on the exit surface. The calculated results were close (within ~ 60 μm) to the experimental results. The lowest HAZ value of 707 μm and surface roughness of 2.43-μm surface roughness were achieved in cutting Type 1 (+ 45°/− 45°) configuration. High-resolution SEM and optical micrographs showed that cracks, cavities, delamination, and matrix decomposition were the typical defects observed in CW fiber laser cutting of CFRP laminates.

Keywords Fiber laser cutting · CFRP · Surface morphology · HAZ

1 Introduction

The use of carbon fiber reinforced plastic (CFRP) composites has shown a marked increase in recent years, particularly in the aerospace and automotive industry due to its relatively high specific strength and stiffness. With increasing application of CFRP materials, machining technology is becoming more important and being the hot research topic. Researchers are devoting to develop an efficient and high-quality process to promote the application of CFRPs. Currently, conventional machining processes including milling, drilling, and turning are mainly used for cutting CFRP composites. Mechanical cutting is the most widely used process but relatively, high level of cutting force, severe tool wear, and workpiece delamination are the challenges [1, 2]. Non-conventional machining methods have also been investigated. For instance, waterjet machining has received considerable attention, which hardly produces significant heat damage or distortion but it leads to moisture absorption or material delamination [3–5].

Laser cutting is preferred to cut heterogeneous materials composed of different phases, because it is non-contacting and non-abrasive machining progressing exhibiting unique advantages, eliminating tool wear, vibrations, and cutting forces [6]. Apart from the general composites, laser cutting has also been applied for cutting nanocomposites and sandwich composites [7, 8], but there are some heat damage generated in laser beam machining of CFRP, such as heat-affected zone (HAZ), matrix recession, delamination, fiber charring, and kerf taper [9]. Many scholars have been investigating these defects and studying for optimal parameters or a novel method to improve quality and efficiency. Mathew et al. [10] used response surface methodology (RSM) to study optimal parameters producing minimal defects in pulsed Nd:YAG laser cutting of CFRP. They found that the parameters including a cutting speed of 0.5–0.8 mm/s, pulse energy of 1.5–2 J, pulse duration of 0.4–0.7 ms, pulse repetition rate of 35–45 Hz, and gas pressure of 5–7 kg/cm^2 could obtain superior

✉ Xujing Yang
yangxujing@hnu.edu.cn

[1] State Key Laboratory of Advanced Design and Manufacture for Vehicle Body, Hunan University, Changsha 410082, Hunan, China

[2] Hunan Provincial Key Laboratory of Intelligent Laser Manufacturing, Hunan University, Changsha 410082, Hunan, China

cut quality for woven carbon fiber reinforced plastic composites with 2-mm thickness. Muramatsu et al. [11] analyzed the effect of three types of laser on cutting 2-mm-thick CFRP and concluded that the most critical way to increase mechanical properties of materials was to reduce the dimension of HAZ. Li et al. [12] found that short laser wavelength could produce less thermal damage. The energy deposited in the material was removed as kinetic energy of the removed particles and hence, there was not very much thermal input, as high photon energy (UV) laser beams could be strong enough to break the molecular bonds in the matter (particularly organic materials). Leone et al. [13] found that the multi-passes scan method could obtain a narrow kerf and limited HAZs because the time passing between two consecutive scans was helpful to cool down the samples. Besides, another method to decrease HAZ is to shorten the pulse duration, which could achieve a high peak power. Gräf et al. [14] used the laser with a very short pulse duration of about 300 ns to keep HAZ below 20 μm. When using a femtosecond and picosecond laser to cut a composite, spot overlap ratio, laser power and scanning speed are the significant factors related to machined quality [15, 16]. The strategies of short laser wavelength and multi-pass and short pulse duration could decrease heat defect, but they were inefficient because they all required a large number of passes to cut through. Cenna et al. [17] presented that the important parameter, energy per unit length (P/v), had a great impact on laser cutting. The energy per unit length (P/v) decided whether the CFRP could be cut through. In addition, with the high energy per unit length, the materials absorbed more heat so that the charred material formed a thick layer, which covered the cut surfaces completely. Negarestani et al. [18] found that the energy per unit length value 17 J/mm was the optimal parameter for the single-pass cutting experiment to obtain the high cutting quality with a continuous wave beam laser. Riveiro et al. [19] explained protruding fibers, charring layer, the dependence of the fiber orientation on the damage of the material, and the influence of laser power during the CO_2 laser processing in a CW mode. By comparing laser with milling and waterjet cutting, Herzog et al. [20] found that tensile strength of samples processed with the three cutting technologies was similar. The utilization of a laser with high beam quality to machine CFRP composites could effectively process with a minimal HAZ and practically not affecting the mechanical properties of the workpiece.

In this work, a high-power fiber laser was employed for all trials, which offers the possibility of delivering the beam in a continuous wave to observe and analyze related machining defects. A fiber laser is superior in certain applications and shows many advantages in terms of stable operation, simplicity, high beam quality under severe environment, and high output power from a simple optical fiber. The characteristic of cutting CFRP with different fiber orientation/lay-up configuration using a fiber laser was studied. The relationship between machining parameters and cutting quality was investigated. The formation of heat damage relating to varying cutting parameters was also explained.

2 Experimental work

2.1 Workpiece material

CFRP laminates manufactured by a high-pressure resin transfer molding (HP-RTM) process with three different configurations/fiber orientations were employed. The schematic structures of CFRP materials are shown in the Fig. 1. These involved Type 1 and Type 2 laminates comprising eight fiber plies with a thickness of 2.0 mm and fiber orientation of + 45°/− 45° and 0°/90° respectively, whereas Type 3 laminate consists of four plain woven fiber plies (lay up in the same direction) also in 2.0 mm thick. The CFRP laminates were made of high-tensile strength carbon fiber (supplied by Toray) impregnated with AM8930A/B epoxy resin (supplied by Wells Advanced Materials) having a fiber weight fraction of 45%. The HP-RTM process was running at 120 °C for injecting resin and then holding for 240 s for curing. Plates measuring 260 mm × 50 mm were cut and prepared for the trials.

2.2 Laser system

A high-power fiber laser was employed in the cutting experiment, which is viewed as a kind of an efficient and high-quality laser emerging in recent years. Experiments were performed by means of a continuous wave IPG YLS-5000 laser. It supplies the maximum output power of 5 kW with a wavelength of 1070 ± 10 nm. Figure 2 shows the laser cutting head and schematic of laser cutting process. The relative movement of the workpiece with regard to the laser beam was achieved by an X-Y-Z CNC laser head. The stand-off was set at 2 mm to put the focus position on the sample surface, which is likely to process a narrow, smooth, and straight kerf [21]. Since the presence of oxygen into the inert gas was shown to have a clear influence on the fiber pull out [18], nitrogen was employed as the assist gas in order to minimize its nature influence on the process.

2.3 Experiment design

All trials were performed using a single-pass cutting strategy for machining a series of 40-mm-long unidirectional straight lines with different variables in order to evaluate the machined quality of different types of CFRP and the effect of cutting parameters. Generally, single-pass processing is the dominant approach in laser cutting applications, which is owing to the maximized material removal rate with minimized operational

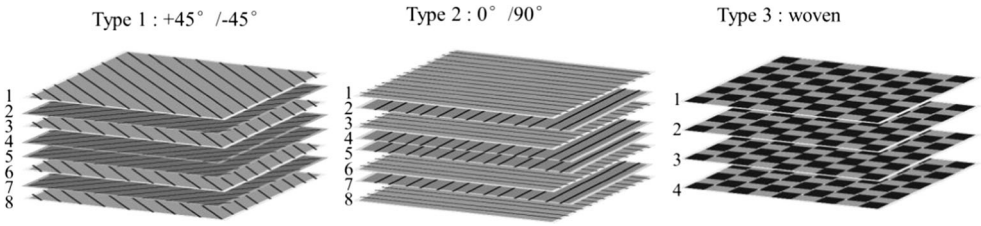

Fig. 1 The schematic structures of CFRP materials

time. The distance between two adjacent cutting lines is ~ 15 mm to ensure maximizing material utilization without HAZ interference. Lower assist gas pressure is preferred, as high pressure (up to 5 bar) promotes large erosion in the entry surface, which can be attributed to the higher dynamic pressure of the jet onto the cutting front.

A full factorial experimental array was employed involving four variable factors, one at three levels and the other three at two levels, giving a total of 24 trials. The factors and corresponding levels are detailed in Table 1. The levels of laser power and cutting speed were selected based on preliminary trials, comprehensive literature review, and theoretical calculation [19, 22–25]. The cutting depth C_d and the width of HAZ (W_h) have a positive correlation with the specific laser energy (also called energy per unit length) [19, 23].

$$W_h \propto \frac{PQ}{v}, C_d \propto \frac{PQ}{v} \tag{1}$$

where P is the laser beam power, v is the cutting speed, and Q is the duty cycle (100% in a CW mode). The formulae of maximum cutting speed with one cutting pass derived from Caprino, G et al. [25] are as follows:

$$v_{\max} = \frac{P}{\delta t_{tot} d} \tag{2}$$

$$\delta = \frac{\pi\beta\rho[H_V + c(T_V - T_0)]}{4\alpha} \tag{3}$$

where P is the laser power, t_{tot} is the thickness of the CFRP, d is the diameter of the beam, β is constant (≈1), ρ is the density, H_v is the specific heat of vaporization, c is the specific heat, T_v is the vaporization temperature, T_0 is the surrounding atmosphere temperature, and the α is the emissivity. δ is a constant for a given material and laser system. For the trials, cutting CFRP with a fiber laser, δ is about 40,000 J/cm^3 and the calculated cutting speed for cutting through samples is around 800 mm/min.

A thermal model was also employed to simulate the dimensions of HAZ and compared with experimental results. ANOVA (analysis of variance) was undertaken using Minitab software to identify the significant factors and levels.

2.4 Sample characterization

The inspection of the entry, exit, and machined surface of the cut was analyzed using a digital microscope (Keyence VHX-5000) with a photographic system in order to record and store the images. For more detailed observations of processed samples from $HAZ_{profile}$, they were cut by a diamond saw and polished using an abrasive paper to analyze the cross section. Quality characteristics evaluated in this work were the width of the heat-affected zone in the entry (HAZ_{entry}), exit (HAZ_{exit}), and profile/cross section ($HAZ_{profile}$), as demonstrated in Fig. 3. Furthermore, machined surface was further studied using high-resolution scanning electron microscopy (SEM). Surface roughness of the cutting direction was measured by a TIME (TR200) surface roughness tester and evaluated with cut-off and evaluation length of 0.8 and 4 mm, respectively.

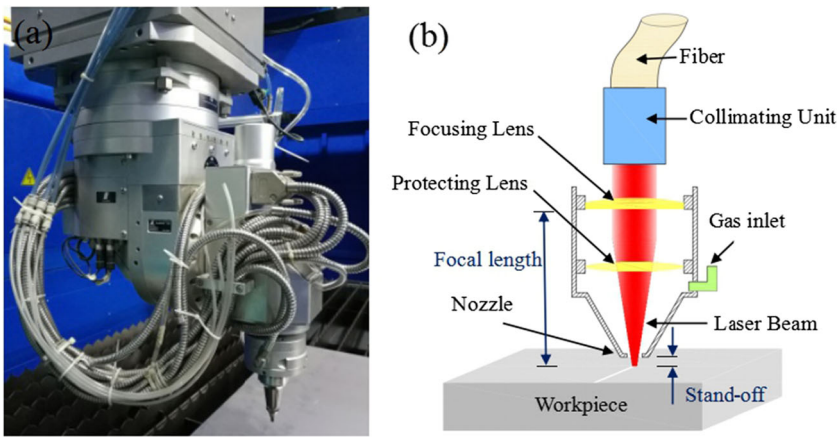

Fig. 2 **a** Laser cutting head and **b** schematic of laser cutting process

Table 1 Experimental factors and their corresponding levels

Factors	Level 1	Level 2	Level 3
Type of material	Type 1	Type 2	Type 3
Cutting speed (mm/min)	600	1000	–
Laser power (W)	650	950	–
Assist gas pressure (bar)	1	4	–

3 Results and discussion

3.1 Heat-affected zone

When focused laser beam impinges on the surface of the workpiece, a certain amount of heat is absorbed by the material at the surface and subsequently was conducted into the workpiece. Heat conduction into the workpiece causes heat damage and deterioration of the material properties to a certain area and depth. Figure 4 shows the typical entry side surface morphology of CFRP laminates with different fiber orientation interacted with a laser beam. All the three trials were conducted using the same processing parameters (600 mm/min, 650 W, 4 bar). Relative smooth cutting edge at the entry side was observed for samples with both Type 1 (+ 45°/− 45°) and Type 2 (0°/90°) fiber orientations, while a large number of protruding fibers were found on the cut for Type 3 (woven) laminates. Nearby the cutting edge, it was observed that the fibers were hardly altered but resin was chemically degraded in all samples. This was most likely due to different thermal response of fibers and resin to the heat input, especially the thermal properties including vaporization temperature and conductivity. Carbon fibers are normally vaporized at ~ 3300 °C, while resin is decomposed at ~ 360 °C. Most areas around the cutting edge showed that fibers were intact but resin was degraded. Besides, heavy coating of resin recast layer and some deposits around the cutting edge were observed in all trials with maximum width of ~ 1500 μm, which was due to the blowing effect from the high pressure (up to 4 bar) assist gas as well as decomposed matrix molten below the laser irradiated surface. HAZ_{entry} levels were relatively consistent with fiber orientated at + 45°/− 45° (Type 1) and 0°/90° (Type 2), while this phenomenon was not recorded for all the trials running with woven laminates (Type 3). It was the result of a clear dependence of the fiber orientation on the thermal damage of the material.

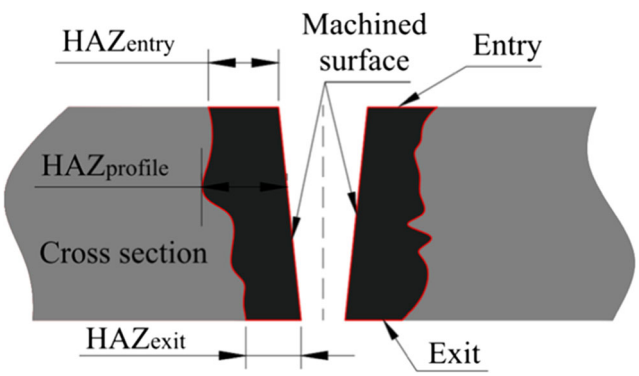

Fig. 3 Scheme of the quality features evaluated to determine the cut quality: heat-affected zone in the entry (HAZ_{entry}), exit (HAZ_{exit}), and cross section/profile ($HAZ_{profile}$)

A small gap (material defect) with the width of ~ 300 μm was found in Fig. 4b, which was possibly due to the uneven configuration of fiber fabric generated in the preforming of the HP-RTM process. As a result, the level HAZ_{entry} of this area rapidly decreased. Another type of defect for woven structure, in contrast to Type 1 and Type 2 configurations, was that the fibers closed to the kerf were easily pulled out. This was possibly due to the uneven heat transfer process in the weave structure laminate. As continuous fibers were cut by the laser together with matrix degradation, fibers were pulled out by the assist gas without bonding strength provided by matrix resin.

HAZ_{exit} recorded in the exit layer were more apparent than the entrance layer. Fiber burrs were observed for all trials due to resin degradation resulting in the lack of bonding strength. On the exit side of the cutting edge, drops of melted resin were observed and located at the further side of HAZ boundary, as there was limited assist gas accessing/passing through to the exit layer of the laminated. The decomposed matrix was not blown away but was attached to the HAZ boundary as a result of no gas pressure effect on the back. For the three types of materials, the HAZ_{exit} was discontinuous, as typically shown in Fig. 5. For the workpiece materials orientated at + 45°/− 45° (Type 1) and 0°/90° (Type 2), it was most likely due to the gap/material defect generated in a fabric preforming process, but a different fiber direction was the main reason for woven samples. HAZ_{exit} recorded perpendicular to fibers was smaller than parallel to fibers because of a different thermal conductivity in a different direction. Similarly, protruding fibers were also observed in the woven material as shown in Fig. 5c, but the number of fibers decreased because of the lower gas pressure reaching the bottom side.

Figure 6 shows $HAZ_{profile}$ of the samples recorded in the cross section, which can be clearly identified regarding to decomposed matrix. The maximum value of $HAZ_{profile}$ was generally recorded between the top and bottom side of the laminates rather than on the top layer. During the laser interacting with workpiece materials, heat was accumulated within the composites and it took relatively longer time to dissipate. It is also apparent that the level of $HAZ_{profile}$ was higher along the fiber orientation. Fiber pullout was also observed on the machined surface, which was caused by the selective removal of the binder matrix relating to decomposition, vaporization, or melt shearing. Carbon fibers without the matrix bonding were easily blown out by the assist gas.

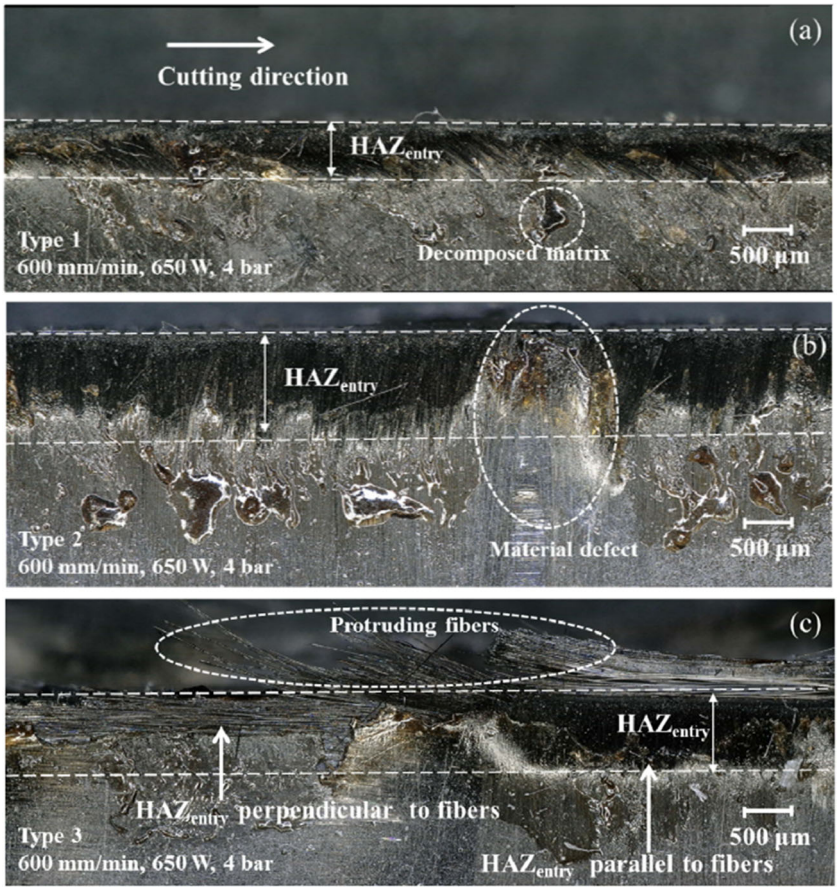

Fig. 4 Entry surface morphology in laser cutting with fiber orientation of **a** + 45°/− 45°, **b** 0°/90°, and **c** woven

3.2 Thermal model analysis

In order to better understand HAZ measurements from the experimental trials, a thermal model describing the transient thermal phenomena near to the cutting edge was employed. The thermal model used in the paper was a simplified model based on the assumption that the laser beam energy was sufficient to cut through the sample. The amount of heat flow and the propagation mode depended on the maximum temperature reached at the boundary zone between the vapor column and the edge, and also the thermal properties of the material. Other assumptions are (a) the thermal flow is unidirectional and perpendicular to the cut; (b) the temperature of the cutting surface is constant during the permanence time (interaction time) of the laser beam on each zone; (c) the lamina is semi-infinite in the direction perpendicular to the cut; (d) the thermal properties of the material do not vary with the temperature.

The governing equation of heat conduction can be written as:

$$k\nabla^2 T + q = \rho_C \frac{\partial T}{\partial t} \tag{4}$$

where k is the thermal conductivity, T is the temperature, q is a heat source term, and c is the specific heat capacity. For a semi-infinite anisotropic body with orthotropic material properties coinciding with the axes of the coordinate system, this equation can be written as:

$$k_x \frac{\partial^2 T}{\partial x^2} + k_y \frac{\partial^2 T}{\partial y^2} + k_z \frac{\partial^2 T}{\partial z^2} + q = \rho_C \frac{\partial T}{\partial t} \tag{5}$$

where k_x, k_y, and k_z are principal conductivities.

Tagliaferri et al. [9] assumed that heat conduction was unidirectional and perpendicular to the cut. The workpiece was also assumed to be semi-infinite in the direction perpendicular to the cut and the thermal properties were assumed to be independent of temperature. The problem of laser cutting was then reduced to one directional heat conduction equation for which a solution was obtained by the finite difference method.

$$\frac{\partial^2 T}{\partial x^2} = \alpha \frac{\partial T}{\partial t} \tag{6}$$

For a one-dimensional array of n nodes with uniform spacing perpendicular to the cut, it becomes

$$T_n^{t+1} = T_n^t \left(1 - \frac{2\alpha \Delta t}{\Delta x^2}\right) + \frac{\alpha \Delta t}{\Delta x^2}\left(T_{n-1}^t - T_{n+1}^t\right) \tag{7}$$

where T_n^t is the temperature at node n and time t, α is the thermal diffusivity of the material, and Δt is the time increment. If the boundary temperature and duration time are recorded, Eq. 7 can be applied to predict the one-dimensional HAZ.

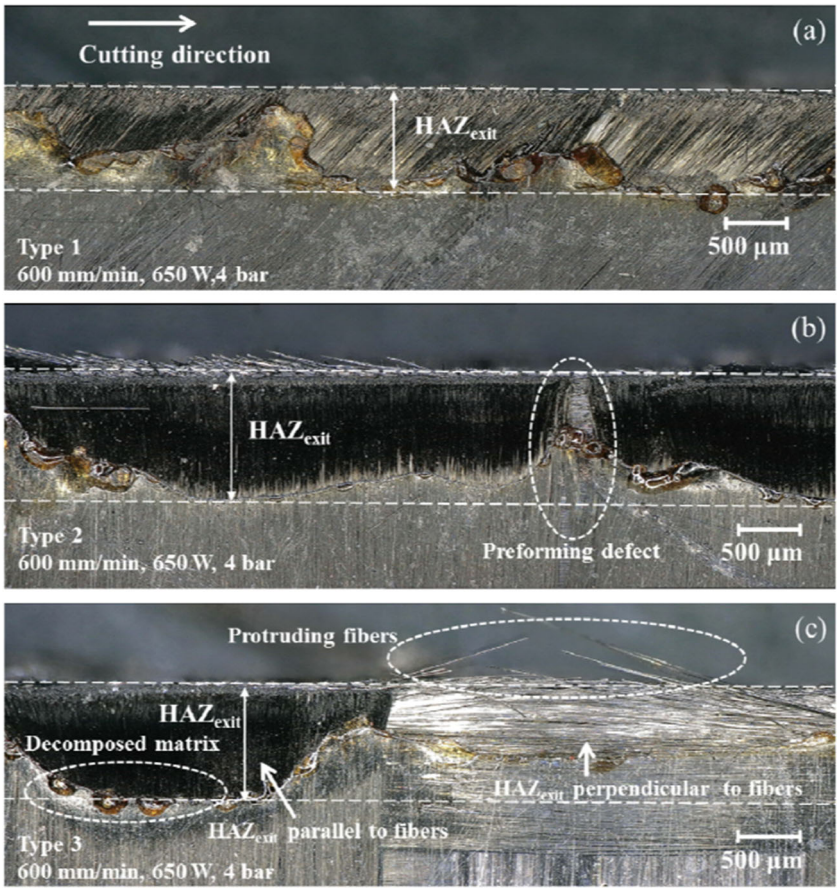

Fig. 5 Exit surface morphology in laser cutting with fiber orientation of **a** + 45°/− 45°, **b** 0°/90°, and **c** woven

In order to accurately simulate heat dissipation in laser machining, Chen et al. [26] developed an explicit three-dimensional finite difference solution for Eq. 5 in laser drilling of carbon/PEEK composites. It was assumed that the laser beam had a Gaussian distribution, material removal took place by vaporization, and heat loss due to radiation was negligible. The upper and lower surfaces of the workpiece were assumed to exchange heat with the environment by heat convection. The governing finite difference equation and the heat convection boundary condition are given by

$$k_x \frac{T^n_{i-1,j,k} - 2T^n_{i,j,k} + T^n_{i+1,j,k}}{\Delta x^2} + k_y \frac{T^n_{i,j-1,k} - 2T^n_{i,j,k} + T^n_{i,j+1,k}}{\Delta y^2} + k_z \frac{T^n_{i,j,k-1} - 2T^n_{i,j,k} + T^n_{i,j,k+1}}{\Delta z^2} + q = \rho c \frac{T^{n+1}_{i,j,k} - T^n_{i,j,k}}{\Delta t} \tag{8}$$

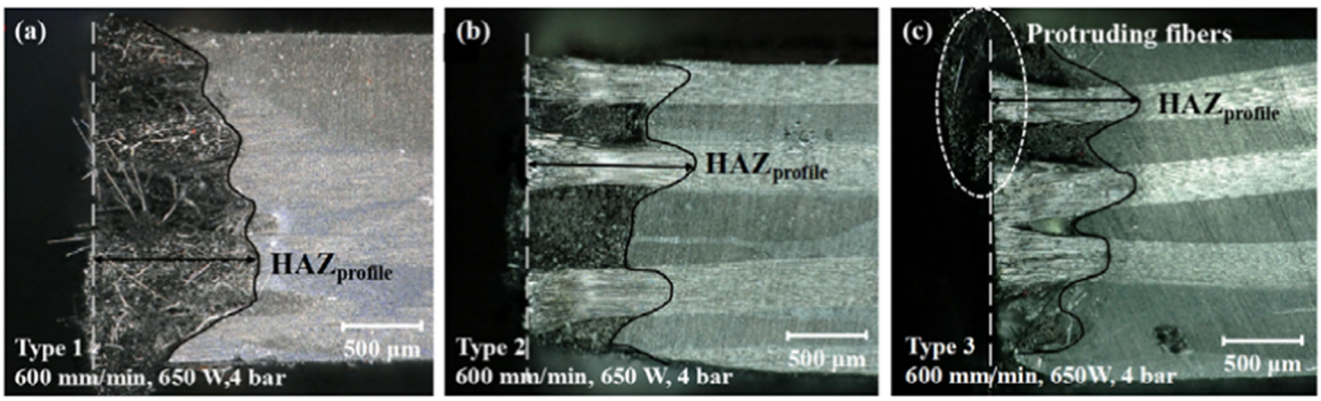

Fig. 6 Optical image of cross section to the cut edge of samples with fiber orientation of **a** + 45°/− 45°, **b** 0°/90°, and **c** woven

where:

$$T_{(x,y,z,t)} = T^{n}_{i,j\cdot k} \tag{9}$$

Applying the three-dimensional model (Eq. 8) based on the method from Tagliaferri et al. [9], it can predict the dimension of HAZ. The schematic depiction of the model is shown in Fig. 7.

The permanence time of the laser beam on each zone of the material (t_i) is connected with the cutting velocity, v, through the relationship:

$$t_i = {}^{d}\!/_{v} \tag{10}$$

where d is the diameter of the beam and the v is the cutting speed. The assumption is that the temperature of the kerf boundary is the vaporization temperature of carbon fiber. Therefore, $T_{0,0,z} = \sim 3300^{\circ}C$. All surfaces are set to convective heat exchange and thermal radiation. The coefficient of convection heat transfer is $h = 50$ [26] and $\varepsilon = 0.8$ [27]. The typical thermal properties of epoxy, carbon fiber, and CFRP are detailed in Table 2 [26, 28]. When the cutting speed is set at 600 mm/min, t_i is around 0.1 s. The maximum temperature along with x direction and corresponding simulation are shown in Fig. 8. The decomposition temperature of epoxy resin is ~360 °C from thermal gravimetric analysis (TGA) [28]. The calculated value of x is 1.05 mm within the thermal model.

The value of 1.05 mm can represent the width of the HAZ for cutting CFRP when fiber orientation is perpendicular to the cut kerf. Therefore, from the simplified thermal model, the HAZ for the exit surface (HAZ_{exit}) of Type 2 (0°/90°) is about 1.05 mm. Through projective relationship, the HAZ for the exit surface of Type 1 (+45°/−45°) lay-up configuration is about $1.05\ \sqrt{2} = 0.75$ mm. However, it is difficult to calculate HAZ levels for Type 3 CFRP (woven) laminated via the thermal model due to the complex fiber orientation and interlayer relationship.

3.3 Statistical analysis

Figure 9 shows the results of HAZ_{entry}, HAZ_{exit}, and $HAZ_{profile}$ measurements with variable cutting parameters. In terms of the level of HAZ_{entry} shown in Fig. 9a, the values were 326–477 μm and 605–940 μm with small variations for Type 1 and Type 2 (+45°/−45° and 0°/90°) materials, respectively. A relatively big variation (~1300 μm) however was found for cutting Type 3 workpiece (woven), especially at the laser power of 950 W irrespective of other two cutting parameters, with the maximum value of ~1900 μm. The result shows that HAZ_{entry} recorded in Type 3 workpiece is more changeable to the heat input.

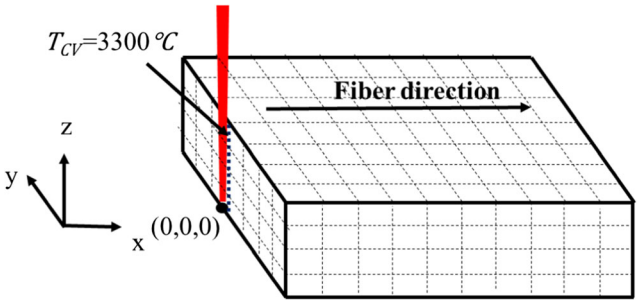

Fig. 7 The schematic depiction of the thermal model

Surprisingly, HAZ_{exit} values recorded at the exit side were almost constant regarding to specific type of CFRP laminate according to Fig. 9b, while the highest level was recorded for Type 2 (0°/90°, up to ~1220 μm) with the lowest level for Type 1 workpiece (+45°/−45°, down to ~650 μm). This was possibly due to the relatively fast heat conduction speed along 0°/90° fiber orientation. Lower value of HAZ was recorded for all trials at the cutting speed of 1000 mm/min. It was understandable that less heat accumulated with higher cutting speed. There was no apparent trend for $HAZ_{profile}$ within the three types of workpiece materials, as shown in Fig. 9c. The highest value (~1400 μm) was recorded using Type 3 workpiece (woven) with the cutting speed and laser power of 600 mm/min and 950 W, respectively.

ANOVA method was applied to further analyze the statistical significant factors and related PCR (percentage contribution ratio) for the HAZ_{entry}, HAZ_{exit}, and $HAZ_{profile}$ values, as shown in Table 3. The factors of assist gas pressure and cutting speed did not appear to have any noticeable effect on HAZ_{entry}, but the type of workpiece and laser power were significant, with a PCR of 46.30% and 14.24% respectively. The results from the ANOVA table also confirmed that the type of workpiece, laser power, and cutting speed were all the statistically significant factors affecting HAZ_{exit} and $HAZ_{profile}$ when applying CW fiber laser cutting of CFRP laminates, with corresponding PCRs varying from 8.32 to 59.61%. The increase in HAZ values was attributed to the greater heat generated during the laser-CFRP interacting process. This was possibly further exacerbated by imperfections or deviations in the surface shape or geometry (e.g., fiber protruding, resin degradation, and microcracks). Surprisingly, it seems that the factor of assist gas pressure had marginal effect on HAZ irrespective the measured position, which was most likely due to huge heat generated in laser cutting process and rapid conduction within fibers. According to the statistical results, the type of workpiece was the main factor for all recorded HAZ; it can be concluded that heat transfer is closely related to the fiber orientation and stacking sequence of manufactured laminates.

Figure 10 shows the detailed information concerning main effects plots for three HAZs recorded at the entry, exit, and cross section, respectively. Expect cutting speed for HAZ_{entry},

Table 2 Typical thermal properties of epoxy, carbon fiber and CFRP [26, 28]

Material	Conductivity (W/m K)	Heat capacity (J/kg K)	Vaporization temperature (°C)	Thermal diffusivity (cm^2/s) × 10^{-3}	Heat of vaporization (J/g)	Density (g/cm^3)
Epoxy	0.2	1100	400	1.2	1100	1.2
Carbon fiber	10	710	3300	380	43,000	1.8
CFRP	$k_x = 5$ $k_y = k_z = 0.5$	950	–	–	–	1.4

the factors including type of workpiece, assist gas pressure, and cutting speed have significant effects on all recorded HAZ. With lower power level and higher cutting speed, all measured HAZ values were relatively small, which was in line with the results reported by Staehr [22]. This is due to decreased power density and the interaction time between the laser and material. It was suggested that a higher laser power and smaller cutting speed exerted more heat at the cutting kerf. A low level of laser power reduced the amount of heat absorbed by the material, and high speed decreased the interaction time between the laser and workpiece material. Although the assist gas pressure was not the main effect factor, increasing the assist gas pressure was also found to decrease the size of heat damage in laser machining. This was possibly attributed to efficient cooling effects of the assist gas. According to the main effects plot together with optical micrographs of the HAZs, it was suggested that HAZ was minimized when employing Type 1 material (+45°/− 45°) with the assist gas pressure, laser power, and cutting speed at 4 bar, 650 W, and 1000 mm/min, respectively.

3.4 Machined surface morphology

Sample surface morphology and several imperfections in the machined surfaces cutting with a CW fiber laser are shown in Fig. 11. Microcracks, craters, and delamination were evident on the machined surface. This fact was probably due to thermal stresses and the pressure of the assist gas, which means that the gas resulting from the ablation process is enclosed under a high pressure due to the volumetric expansion during the vaporization of a solid material. The stress for the CFRP is limited in a range so that delamination or craters are often the consequence [29]. Decomposed matrix in yellow color was apparent, which was due to the resin absorbing laser energy to melt and then sticking to the cross section. Some unique defects occurred after the processing indicated a clear dependence of the fiber orientation and stacking sequence on the damage of the material. Severe collapses were found on the machined surfaces of Type 2 workpiece, and protruding fibers were prevalent for Type 3. Microcracks were more pronounced in samples with +45°/− 45° fiber orientation (Type 1). This fact was probably due to the residual stress because of different thermal response of the fibers and resin together with thermal decomposition and vaporization of matrix material. A relatively uniform surface finishing was observed with Type 1 workpiece material.

The surface morphology obtained after cutting indicated a clear dependence of the fiber orientation and cutting parameters on the thermal damage. Scattered irregular formation of structures together with microcracks around the fiber tips was found when cutting woven CFRP laminates, as shown in Fig. 12a, which was highly related to the cutting speed (1000 mm/min) owing to repeated drilling event. Delamination was significantly reduced with the increase of speed, because the interaction time between the laser and material was reduced. For the trials running with high

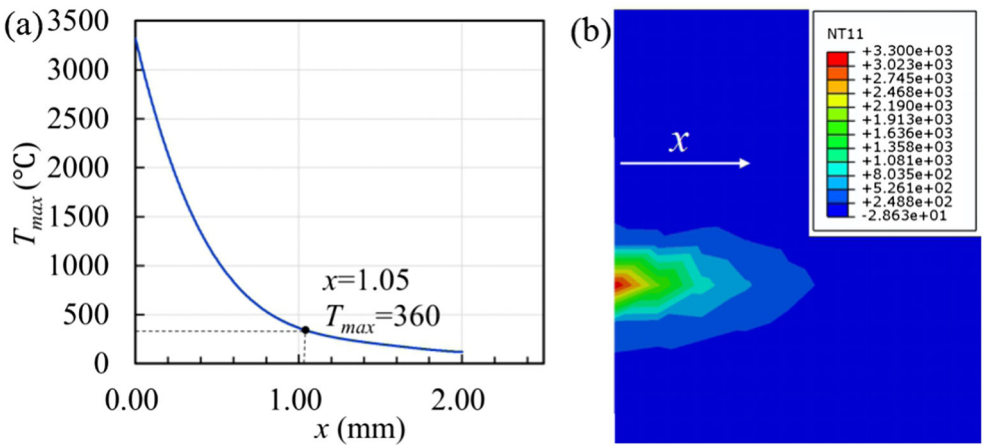

Fig. 8 **a** The maximum temperature decreases with increasing *x* and **b** predicted thermal field at the cutting speed of 600 mm/min

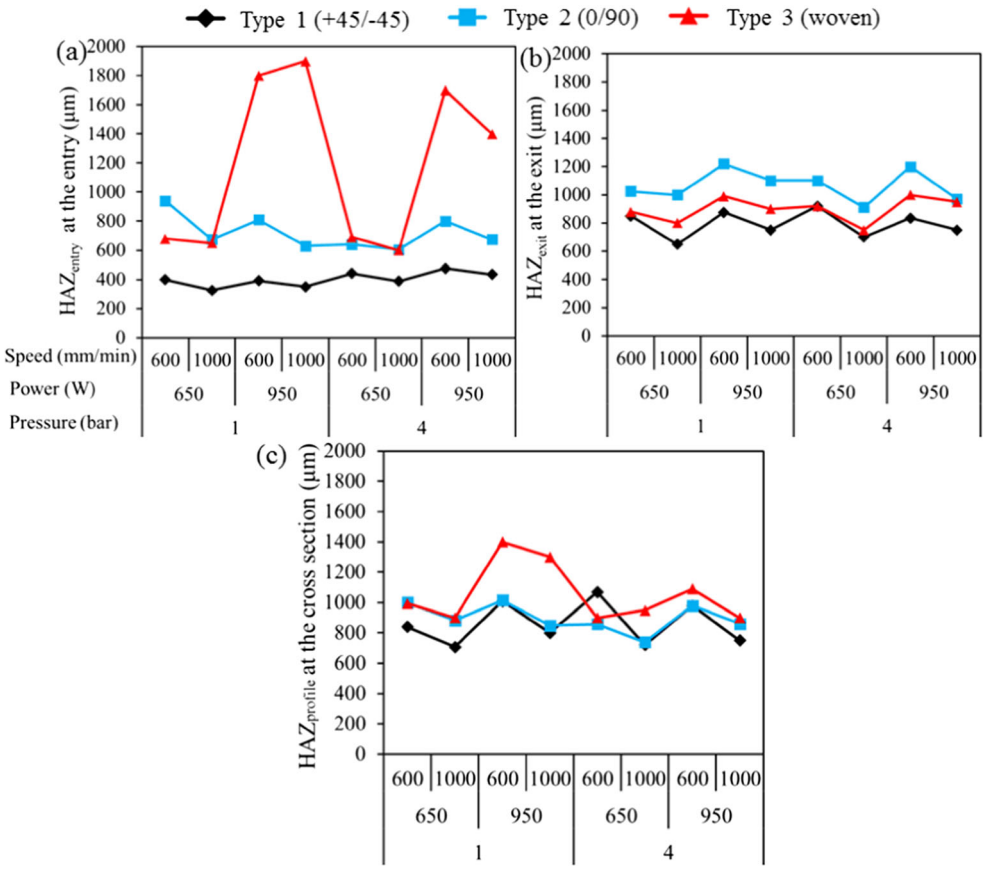

Fig. 9 Measurement results of **a** HAZ_{entry}, **b** HAZ_{exit}, and **c** $HAZ_{profile}$ after laser cutting of different CFRP laminates

speed (1000 mm/min) and power level (950 W), decomposed matrix in yellow color was apparent as shown in Fig. 12b, which was due to the resin absorbing laser energy to melt and then sticking to the cuts. This phenomenon was also deteriorated when running with relatively low assist gas pressure (1 bar).

The laser cutting surfaces were further analyzed using a high-resolution SEM microscope. As shown in Fig. 13a, b, several microcracks were observed along the cutting direction. The machined surface was covered with melted resin. According to Fig. 13c, d, surface morphology was highly related to the machined position. Several small porosities

Table 3 ANOVA results for the HAZ_{entry}, HAZ_{exit}, and $HAZ_{profile}$

	Source of variances	D.F.	Adj. S.S.	Adj. M.S.	*F*	PCR
HAZ_{entry}	Workpiece material	2	2,432,363	1,216,182	13.82*	46.30%
	Assist gas pressure	1	20,417	20,417	0.23	0.00%
	Laser power	1	781,926	781,926	8.88*	14.24%
	Cutting speed	1	53,771	53,771	0.61	0.00%
	Residual	18	1,584,527	88,029		39.46%
	Total	23	4,873,004			100%
HAZ_{exit}	Workpiece material	2	305,827	152,914	56.48*	59.61%
	Assist gas pressure	1	51	51	0.02	0.00%
	Laser power	1	44,634	44,634	16.49*	8.32%
	Cutting speed	1	104,676	104,676	38.66*	20.23%
	Residual	18	48,735	2708		11.83%
	Total	23	503,924			100%
$HAZ_{profile}$	Workpiece material	2	170,119	85,059	6.83*	22.74%
	Assist gas pressure	1	33,750	33,750	2.71	3.34%
	Laser power	1	78,433	78,433	6.30*	10.33%
	Cutting speed	1	132,017	132,017	10.60*	18.73%
	Residual	18	224,186	12,455		44.86%
	Total	23	638,504			100%

*Significant at the 5% level, $F_{0.05,\ 2,\ 18} = 3.55$, $F_{0.05,\ 1,\ 18} = 4.41$

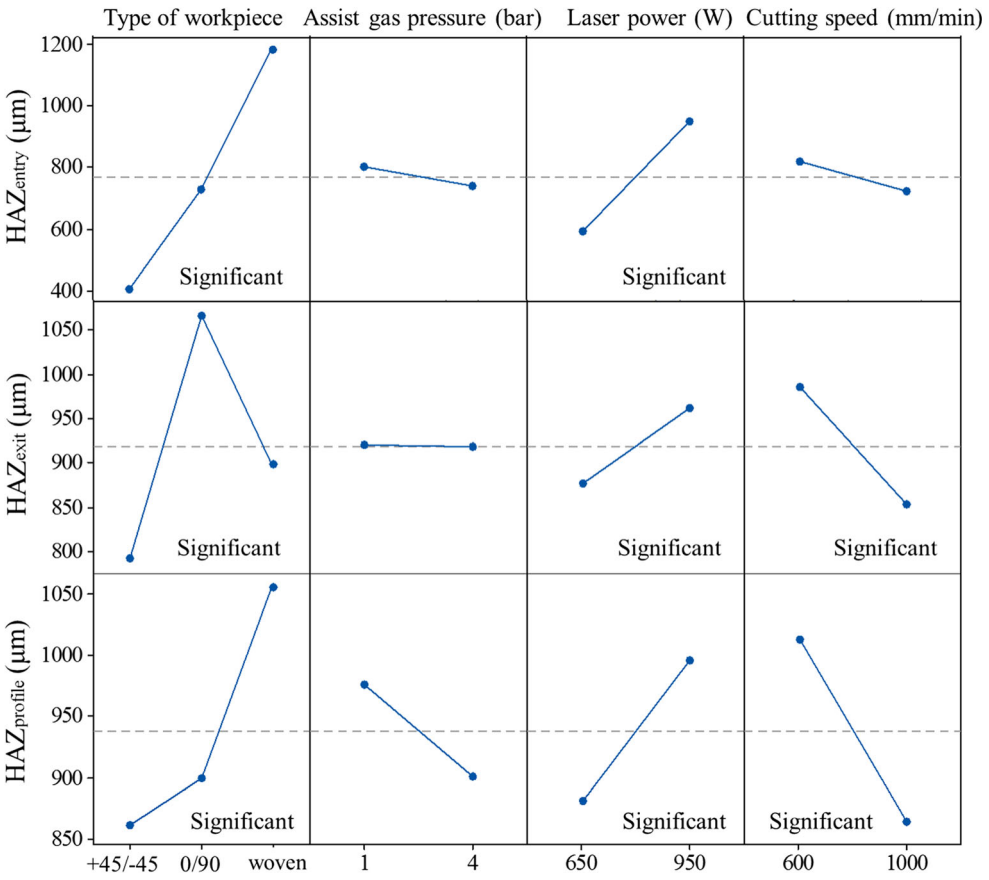

Fig. 10 Main effects plot for HAZ_{entry}, HAZ_{exit}, and $HAZ_{profile}$

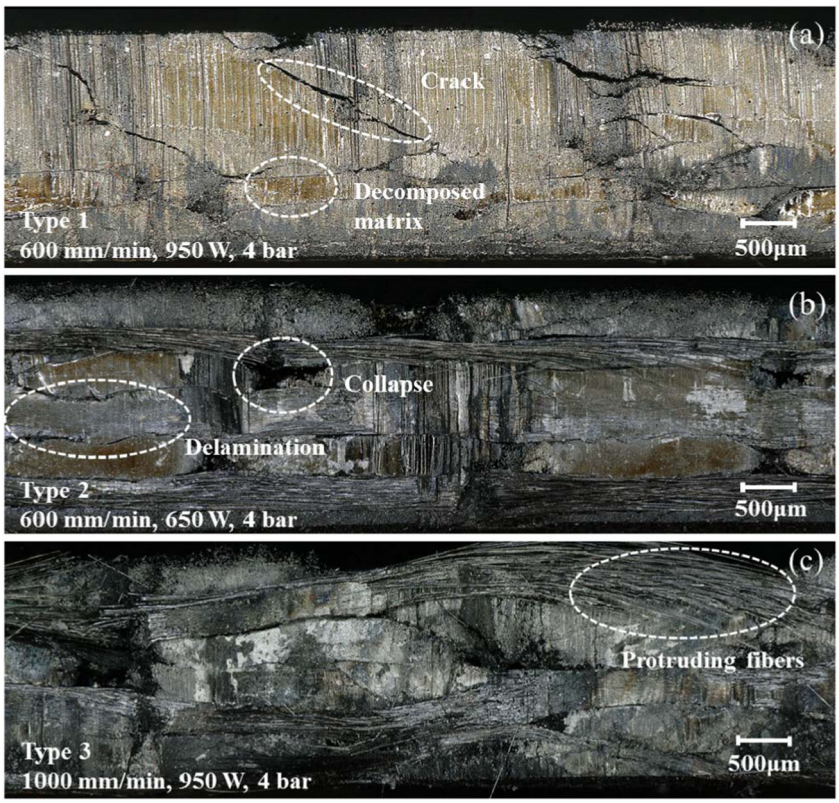

Fig. 11 Surface morphology of machined surface in laser cutting with fiber orientation of **a** + 45°/− 45°, **b** 0°/90°, and **c** woven

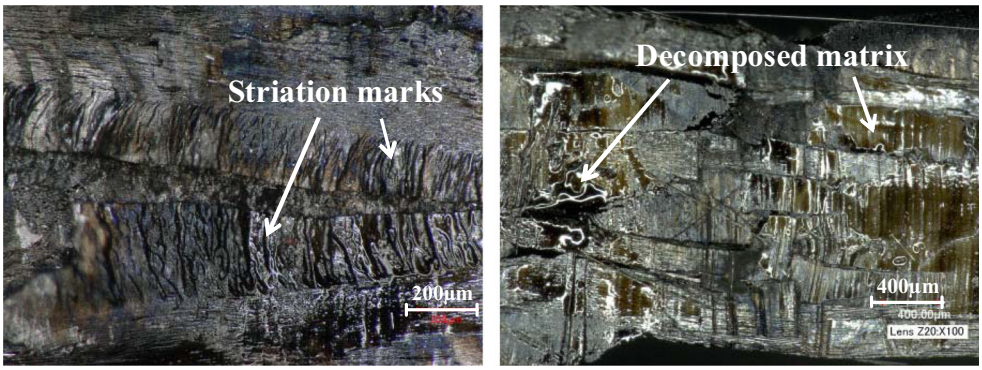

Fig. 12 Optical image of machined surface for cutting woven samples with different parameters **a** 1000 mm/min, 650 W, 1 bar and **b** 1000 mm/min, 950 W, 1 bar

were distributed between fibers observed near the entry surface, which was probably due to the fact that the resin has been decomposed, removed by assist gas, and then cavities were formed and created. However, the surface located next to the exit side was relatively compact rather than porous between fibers. The zone near the exit hardly affected by assist gas was easy to accumulate heat, which led to swelling of fiber ends. Then, fiber swelling squeezed the matrix into a small sectional area and the circle section also turned into a hexagon feature [26]. Most area of laser machined surfaces was covered with resin and fiber fragments, as shown in Fig. 14d.

3.5 Surface roughness

Figure 14 details the surface roughness (Ra) values for all trials, which ranged between 2.43 and 7.63 µm depending on laser cutting parameters and fiber orientation. The minimum Ra was recorded in the trial using Type 1 (+ 45°/− 45°) workpiece with the cutting speed, laser power, and assistant gas pressure at 600 mm/min, 650 W, and 4 bar, respectively. This was possibly attributed to relatively less heat input, and melted resin covered the machined surface. Generally, cutting + 45°/− 45° fiber orientated CFRP laminates shows superior surface roughness (Ra) compared with other two types of

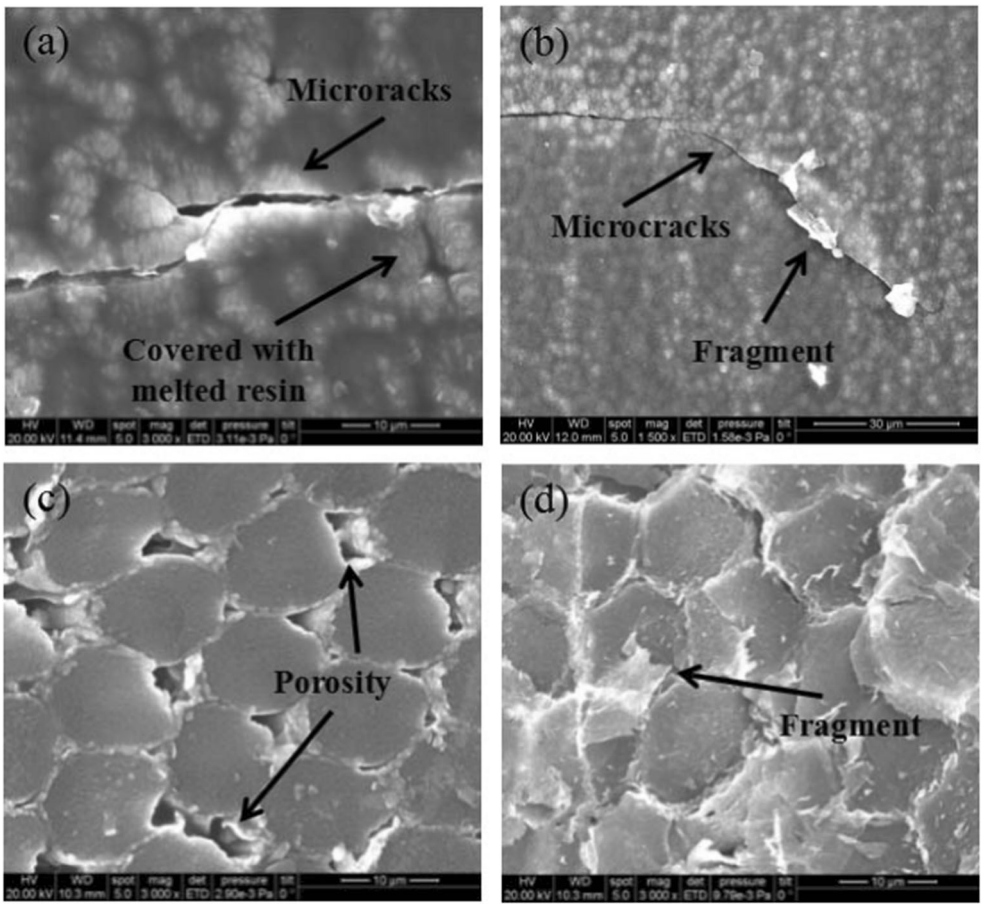

Fig. 13 High-resolution SEM images of machined surface with different morphology running at 1000 mm/min, 650 W, and 4 bar for **a** Type 1 (+ 45°/− 45°), **b** Type 2 (0°/90°), **c** Type 1 (+ 45°/− 45°) at the entry side, and **d** Type 1 (+ 45°/− 45°) at the exit side

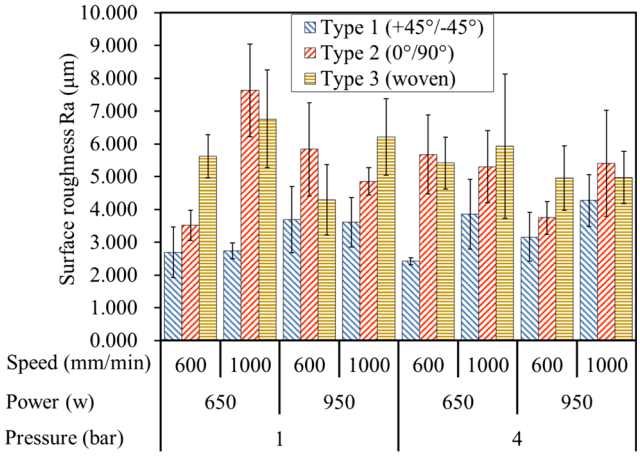

Fig. 14 Surface roughness (Ra) values recorded for all trials

laminates. The trends however were not apparent between fibers orientated at 0°/90° and woven irrespective of cutting parameters. This was due to different volume of heat conducted inside the materials, which was in line with HAZ measurements. According to statistical analysis, the main effects plot suggested that the preferred combination for obtaining lower Ra was running at a cutting speed of 600 mm/min, laser power of 950 W, and assistant gas pressure of 4 bar with Type 1 workpiece. According to the corresponding ANOVA calculations, workpiece material and cutting speed were significant at the 5% level with regard to Ra values and having a PCR of 51.53% and 9.09%, respectively. Lower cutting speed was preferred for cutting CFRP laminated in terms of Ra, which was due to melted/softened relatively large amount of resin and then cover/recast on the cutting surface. None of the other variables was found to have a major influence on Ra after laser cutting process.

4 Conclusions

The paper presented experimental data relating to heat-affected zone (HAZ) and surface quality when using continuous wave fiber laser cutting of CFRP laminated with different lay-up configurations and parameters. The following conclusions can be summarized from above discussions:

(1) Microcracks, delamination, cavities, and fiber protruding were the typical defects observed following fiber laser cutting of CFRP laminates. Resin decomposition, deposits, and heavy coating of recast layer were the most prominent damage related to matrix materials.
(2) Simplified thermal model was built to simulate HAZ values recorded on the exit surface when cutting multi-directional CFRP laminates. The calculated results were close (within ~ 60 μm) to the experimental measurements for Type 1 and Type 2 CFRP laminates when cutting at the speed of 600 mm/min.
(3) The level of HAZ of laser cut CFRP laminate was highly related to fiber orientation, laser power, and cutting speed. The minimum HAZ value recorded in the cross section was achieved when running at the cutting speed of 1000 mm/min together with laser power of 650 W and 4 bar assist gas.
(4) The type of workpiece and laser power were the significant factor affecting HAZ values irrespective of measuring position (entry, exit, and cross section), while cutting speed was also significant for HAZ_{exit} and $HAZ_{profile}$.
(5) Surface roughness for Type 1 (+ 45°/− 45°) CFRP laminates was found to be lower compared to samples orientated at 0°/90° (Type 2) and woven (Type 3) with the minimum Ra of 2.43 μm. Workpiece material and cutting speed were statistically significant for controlling surface roughness levels with corresponding PCRs of 51.53% and 9.09%, respectively.

Funding The authors would like to appreciate the financial support sponsored by "the Fundamental Research Funds for Central Universities (531107050870)."

References

1. Turki Y, Habak M, Velasco R, Vantomme P (2017) Highlighting cutting mechanisms encountered in carbon/epoxy composite drilling using orthogonal cutting. Int J Adv Manuf Technol 92(1):685–697. https://doi.org/10.1007/s00170-017-0153-0
2. Liu D, Tang Y, Cong WL (2012) A review of mechanical drilling for composite laminates. Compos Struct 94(4):1265–1279. https://doi.org/10.1016/j.compstruct.2011.11.024
3. Shanmugam DK, Nguyen T, Wang J (2008) A study of delamination on graphite/epoxy composites in abrasive waterjet machining. Compos A Appl Sci Manuf 39(6):923–929. https://doi.org/10.1016/j.compositesa.2008.04.001
4. MM IW, Azmi AI, Lee CC, Mansor AF (2018) Kerf taper and delamination damage minimization of FRP hybrid composites under abrasive water-jet machining. Int J Adv Manuf Technol 94:1727–1744. https://doi.org/10.1007/s00170-016-9669-y
5. Shanmugam DK, Chen FL, Siores E, Brandt M (2002) Comparative study of jetting machining technologies over laser machining technology for cutting composite materials. Compos Struct 57(1):289–296. https://doi.org/10.1016/S0263-8223(02)00096-X
6. Sheikh-Ahmad JY (2009) Machining of polymer composites. Springer US, New York
7. Nagesh S, Narasimha Murthy HN, Pal R, Supreeth Dev SD, Krishna M (2017) Investigation of the effect of nanofillers on the quality of CO2 laser cutting of FRP nanocomposites. Int J Adv Manuf Technol 90(5):2047–2061. https://doi.org/10.1007/s00170-016-9535-y

8. Krot K, Chlebus E, Kuźnicka B (2017) Laser cutting of composite sandwich structures. Arch Civ Mech Eng 17(3):545–554. https://doi.org/10.1016/j.acme.2016.12.007
9. Tagliaferri V, Di Ilio A, Visconti C (1985) Laser cutting of fibre-reinforced polyesters. Compos 16(4):317–325. https://doi.org/10.1016/0010-4361(85)90284-8
10. Mathew J, Goswami GL, Ramakrishnan N, Naik NK (1999) Parametric studies on pulsed Nd:YAG laser cutting of carbon fibre reinforced plastic composites. J Mater Process Technol 89–90:198–203. https://doi.org/10.1016/S0924-0136(99)00011-4
11. Muramatsu M, Harada Y, Suzuki T, Niino H (2015) Infrared stress measurements of thermal damage to laser-processed carbon fiber reinforced plastics. Compos A Appl Sci Manuf 68:242–250. https://doi.org/10.1016/j.compositesa.2014.08.033
12. Li ZL, Zheng HY, Lim GC, Chu PL, Li L (2010) Study on UV laser machining quality of carbon fibre reinforced composites. Compos A Appl Sci Manuf 41(10):1403–1408. https://doi.org/10.1016/j.compositesa.2010.05.017
13. Leone C, Genna S, Tagliaferri V (2014) Fibre laser cutting of CFRP thin sheets by multi-passes scan technique. Opt Lasers Eng 53:43–50. https://doi.org/10.1016/j.optlaseng.2013.07.027
14. Gräf S, Staupendahl G, Krämer A, Müller FA (2015) High precision materials processing using a novel Q-switched CO_2 laser. Opt Lasers Eng 66:152–157. https://doi.org/10.1016/j.optlaseng.2014.09.007
15. Salama A, Li L, Mativenga P, Sabli A (2016) High-power picosecond laser drilling/machining of carbon fibre-reinforced polymer (CFRP) composites. Appl Phys A Mater Sci Process 122(2):73. https://doi.org/10.1007/s00339-016-9607-8
16. Liu Y, Zhang R, Li W, Wang J, Yang X, Cheng L, Zhang L (2018) Effect of machining parameter on femtosecond laser drilling processing on SiC/SiC composites. Int J Adv Manuf Technol 96:1795–1811. https://doi.org/10.1007/s00170-017-1163-7
17. Cenna AA, Mathew P (1997) Evaluation of cut quality of fibre-reinforced plastics—a review. Int J Mach Tools Manuf 37(6):723–736. https://doi.org/10.1016/S0890-6955(96)00085-5
18. Negarestani R, Li L, Sezer HK, Whitehead D, Methven J (2010) Nano-second pulsed DPSS Nd:YAG laser cutting of CFRP composites with mixed reactive and inert gases. Int J Adv Manuf Technol 49(5):553–566. https://doi.org/10.1007/s00170-009-2431-y
19. Riveiro A, Quintero F, Lusquiños F, del Val J, Comesaña R, Boutinguiza M, Pou J (2012) Experimental study on the CO2 laser cutting of carbon fiber reinforced plastic composite. Compos A Appl Sci Manuf 43(8):1400–1409. https://doi.org/10.1016/j.compositesa.2012.02.012
20. Herzog D, Jaeschke P, Meier O, Haferkamp H (2008) Investigations on the thermal effect caused by laser cutting with respect to static strength of CFRP. Int J Mach Tools Manuf 48(12–13):1464–1473. https://doi.org/10.1016/j.ijmachtools.2008.04.007
21. Herzog D, Schmidt-Lehr M, Oberlander M, Canisius M, Radek M, Emmelmann C (2016) Laser cutting of carbon fibre reinforced plastics of high thickness. Mater Des 92:742–749. https://doi.org/10.1016/j.matdes.2015.12.056
22. Staehr R, Bluemel S, Jaeschke P, Suttmann O, Overmeyer L (2016) Laser cutting of composites-two approaches toward an industrial establishment. J Laser Appl 28(2):022203. https://doi.org/10.2351/1.4943754
23. Pan CT, Hocheng H (1998) Prediction of extent of heat affected zone in laser grooving of unidirectional fiber-reinforced plastics. J Eng Mater Technol 120(4):321–327. https://doi.org/10.1115/1.2807021
24. Chryssolouris G, Sheng P, Choi WC (1990) Three-dimensional laser machining of composite materials. J Eng Mater Technol 112(4):387–392. https://doi.org/10.1115/1.2903347
25. Caprino G, Tagliaferri V (1988) Maximum cutting speed in laser cutting of fiber reinforced plastics. Int J Mach Tools Manuf 28(4):389–398. https://doi.org/10.1016/0890-6955(88)90052-1
26. Cheng CF, Tsui YC, Clyne TW (1998) Application of a three-dimensional heat flow model to treat laser drilling of carbon fibre composites. Acta Mater 46(12):4273–4285. https://doi.org/10.1016/S1359-6454(98)00090-1
27. Wu CW, Wu XQ, Huang CG (2015) Ablation behaviors of carbon reinforced polymer composites by laser of different operation modes. Opt Laser Technol 73:23–28. https://doi.org/10.1016/j.optlastec.2015.04.008
28. Pan CT, Hocheng H (2001) Evaluation of anisotropic thermal conductivity for unidirectional FRP in laser machining. Compos A Appl Sci Manuf 32(11):1657–1667. https://doi.org/10.1016/S1359-835X(00)00093-2
29. Stock J, Zaeh MF, Conrad M (2012) Remote laser cutting of CFRP: improvements in the cut surface. Phys Procedia 39:161–170. https://doi.org/10.1016/j.phpro.2012.10.026